Multistep Electron Transfer between Porphyrin Modules Assembled around a Ruthenium Center

Anthony Harriman,*,† Fabrice Odobel,‡ and Jean-Pierre Sauvage*,‡

Contribution from the Center for Fast Kinetics Research, The University of Texas at Austin, Austin, Texas 78712, and Laboratoire de Chimie Organo-minérale, Faculté de Chimie, Université Louis Pasteur, 1 rue Blaise Pascal, 67008 Strasbourg, France

Received August 22, 1994. Revised Manuscript Received April 10, 1995®

Abstract: A new strategy has been devised for the construction of photoactive multicomponent arrays based on metal ion chelation whereby bisporphyrins have been assembled around a central ruthenium(II) bis(terpyridyl) complex. One of the terminal subunits is a gold(III) porphyrin while the second terminus is selected from a gold(III), zinc(II), or free-base porphyrin. Photophysical properties have been measured for each of the tripartite compounds using ultrafast transient absorption and emission spectroscopy. Excitation into the central ruthenium(II) bis(terpyridyl) complex is followed by rapid intramolecular triplet energy transfer to one of the appended porphyrins. Direct excitation into the gold(III) porphyrin subunit generates the corresponding triplet excited state which is unreactive toward energy- or electron-transfer processes. In contrast, excitation into the zinc(II) or free-base porphyrin produces the corresponding excited singlet state which transfers an electron to the adjacent ruthenium(II) bis(terpyridyl) complex. Secondary electron transfer to the appended gold(III) porphyrin competes with reverse electron transfer such that the redox equivalents become separated by about 30 Å. The original ground-state system is restored by relatively slow interporphyrin electron transfer. The energetics for each of these electron-transfer steps have been evaluated from electrochemical measurements and by measuring the rates as a function of temperature and solvent polarity. For the zinc(II) porphyrin-containing triad, electron transfer takes place in the solid state at 77 K. Finally, the performance of the latter triad is compared with that of the bacterial photosynthetic reaction center complex.

Introduction

The primary electron-transfer step in bacterial photosynthetic reaction center complexes occurs between porphyrinic species over a center-to-center separation of *ca.* 17 Å.[1] The rate of electron transfer is extremely fast ($k \approx 3 \times 10^{11}$ s^{-1}),[2] despite the fact that there is only a modest thermodynamic driving force ($\Delta G° \approx -0.39$ eV),[3] and only very weakly dependent on temperature.[4] Such behavior is not well reproduced by model systems,[5] although many synthetic systems are able to demonstrate sequential electron transfer between spatially-remote, redox-active subunits.[5-9] Indeed, a key feature of natural photosynthesis involves the weakly exergonic initial photoredox step, which is followed by a series of mildly exergonic electron-transfer reactions, leading to formation of a long-lived, spatially-separated redox pair.[10] Most model systems have been designed so as to ensure a rapid rate of initial electron transfer by virtue of a high driving force.[5] Here, we describe porphyrin-based molecular triads[9] for which the light-induced electron-transfer steps are moderately exergonic and are followed by secondary, more thermodynamically favorable electron-transfer reactions. The system operates well at ambient temperature, and remarkably, electron transfer still proceeds[11,12] in the solid state at 77 K.

This study is an extension of our earlier work[12,13] in which it was established that photoinduced electron transfer from a zinc(II) porphyrin to a covalently-linked gold(III) porphyrin provides a good, albeit crude, model for the primary interporphyrin electron-transfer step in bacterial photosynthesis. In order to

† The University of Texas at Austin.

‡ Université Louis Pasteur.

® Abstract published in *Advance ACS Abstracts*, August 15, 1995.

(1) (a) Deisenhofer, J.; Epp, O.; Miki, K.; Huber, R.; Michel, H. *J. Mol. Biol.* **1984**, *80*, 385. (b) Chang, C. H.; Tiede, D.; Tang, J.; Smith, U.; Norris, J. R.; Schiffer, M. *FEBS Lett.* **1986**, *205*, 82.

(2) (a) Kirmaier, C.; Holten, D.; Parson, W. W. *Biochim. Biophys. Acta* **1985**, *810*, 33; 49. (b) Wasielewski, M. R.; Tiede, D. *FEBS Lett.* **1986**, *204*, 368. (c) Martin, J.-L.; Breton, J.; Hoff, A.; Migus, A.; Antonetti, A. *Proc. Natl. Acad. Sci. U.S.A.* **1986**, *83*, 957. (d) Breton, J.; Martin, J.-L.; Migus, A.; Antonetti, A.; Orszag, A. *Proc. Natl. Acad. Sci. U.S.A.* **1986**, *83*, 5121. (e) Gao, J.; Shopes, R. J.; Wraight, C. A. *Biochim. Biophys. Acta* **1990**, *1015*, 95.

(3) (a) Franzen, S.; Goldstein, R. F.; Boxer, S. G. *J. Phys. Chem.* **1993**, *97*, 3040. (b) Marcus, R. A.; Sutin, N. *Biochim. Biophys. Acta* **1985**, *811*, 265.

(4) (a) Fleming, G. R.; Martin, J.-L.; Breton, J. *Nature* **1988**, *333*, 190. (b) Bixon, M.; Jortner, J. *Chem. Phys. Lett.* **1989**, *159*, 17.

(5) (a) Connolly, J. S.; Bolton, J. R. In *Photoinduced Electron Transfer*; Fox, M. A., Chanon, M., Eds.; Elsevier: Amsterdam, 1988; Part D; p 303. (b) Gust, D.; Moore, T. A. *Science* **1989**, *244*, 35. (c) Maruyama, K.; Osuka, A. *Pure Appl. Chem.* **1990**, *62*, 1511. (d) Wasielewski, M. R. *Chem. Rev.* **1992**, *92*, 435. (e) Sauvage, J.-P.; Harriman, A. *Chem. Soc. Rev.*, submitted for publication.

(6) (a) Ohkohchi, M.; Takahashi, A.; Mataga, N.; Okada, T.; Osuka, A.; Yamada, H.; Maruyama, K. *J. Am. Chem. Soc.* **1993**, *115*, 12137. (b) Osuka, A.; Marumo, S.; Maruyama, K.; Mataga, N.; Tanaka, Y.; Taniguchi, S.; Okada, T.; Yamazaki, I.; Nishimura, Y. *Bull. Chem. Soc. Jpn.* **1995**, *68*, 262.

(7) Gust, D.; Moore, T. A.; Moore, A. L.; Macpherson, A. N.; Lopez, A.; DeGraziano, J. M.; Gouni, I.; Bittersman, E.; Seely, G. R.; Gao, F.; Nieman, R. A.; Ma, X. C.; Demanche, L. J.; Hung, S.-C.; Luttrull, D. K.; Lee, S.-J.; Kerrigan, P. K. *J. Am. Chem. Soc.* **1993**, *115*, 11141.

(8) Brouwer, A. M.; Eijckelhoff, R. J.; Willemse, R. J.; Verhoeven, J. W.; Schuddleboom, W.; Warman, J. M. *J. Am. Chem. Soc.* **1993**, *115*, 2988.

(9) Harriman, A.; Odobel, F.; Sauvage, J.-P. *J. Am. Chem. Soc.* **1994**, *116*, 5481.

(10) (a) Holten, D.; Windsor, M. W.; Parson, W. W.; Thorner, J. P. *Biochim. Biophys. Acta* **1978**, *501*, 112. (b) Nonella, M.; Schulten, K. *J. Phys. Chem.* **1991**, *95*, 2059. (c) Barber, J.; Anderson, B. *Nature* **1994**, *370*, 31.

(11) Gaines, G. L., III; O'Neil, M. P.; Svec, W. A.; Niemczyk, M. P.; Wasielewski, M.R. *J. Am. Chem. Soc.* **1991**, *113*, 719.

(12) Harriman, A.; Heitz, V.; Ebersole, M.; van Willigen, H. *J. Phys. Chem.* **1994**, *98*, 4982.

(13) (a) Brun, A. M.; Harriman, A.; Heitz, V.; Sauvage, J.-P. *J. Am. Chem. Soc.* **1991**, *113*, 8657. (b) Chambron, J.-C.; Harriman, A.; Heitz, V.; Sauvage, J.-P. *J. Am. Chem. Soc.* **1993**, *115*, 6109. (c) Chambron, J.-C.; Harriman, A.; Heitz, V.; Sauvage, J.-P. *J. Am. Chem. Soc.* **1993**, *115*, 7419. (d) Harriman, A.; Heitz, V.; Sauvage, J.-P. *J. Phys. Chem.* **1993**, *97*, 5940.

0002-7863/95/1517-9461$09.00/0

provide for a cascade of electron-transfer events, the porphyrin subunits have now been bridged with a ruthenium(II) bis(terpyridyl) complex.[14] This latter subunit takes several roles: notably, (i) acting as a template to assemble the bisporphyrin, (ii) functioning as a real redox intermediate in forward electron-transfer steps, and (iii) channeling absorbed photons to the appended porphyrin subunits. The molecular triads are compact, with restricted degrees of rotational freedom, and the respective electron-transfer steps correspond to charge-shift reactions as opposed to formal charge separation and recombination. Also, reorganization energies are found to be relatively small. This feature is important because, as in natural photosynthesis,[15] it permits maximization of the rates of electron transfer at low thermodynamic driving force and ensures that charge recombination to re-form the ground state falls well within the Marcus inverted region.[16] Furthermore, the activation energy for forward electron transfer is expected to be close to zero, because of the similarity between driving force and reorganization energy.[17] This feature, taken together with the small reorganization energy, favors photoinduced electron transfer in a low-temperature glass.

Related dyads are known in which a porphyrin is closely-linked to a silver(I),[18] ferrocinium,[19] ruthenium(II),[20,21] rhodium(III),[21] or molybdenum(III)[22] complex, and the photophysical properties have been explored in certain cases. However, it is important to realize the advantages provided by the modular synthetic approach used here to assemble the triads.[14] Both the nature of the terminal porphyrins and the type of cation coordinated at the central chelate can be changed readily. In this way, it might become possible to construct families of triads with individual members possessing distinctive electronic properties. The terminal porphyrins can also be further functionalized so as to accommodate additional terpyridyl complexes, thereby forming linear oligomeric structures.[21]

Experimental Section

Materials. Solvents used for spectroscopic studies were of the highest available commercial grade and were fractionally distilled from appropriate drying agents before use. Pyrrole was purified by distillation under reduced pressure from KOH and dichloromethane was distilled under Ar from P_2O_5, while all other solvents and chemicals were used as received. Porphyrinic derivatives were protected from light by aluminum foil during purification on chromatography columns and during heating. 3,5-Di-*tert*-butylbenzaldehyde,[23] 4′-(4-formylphenyl)-2,2′:6′,2″-terpyridine,[24] and bis(3-ethyl-4-methyl-2-pyrryl)methane[25] were prepared according to literature procedures. Structures of the two

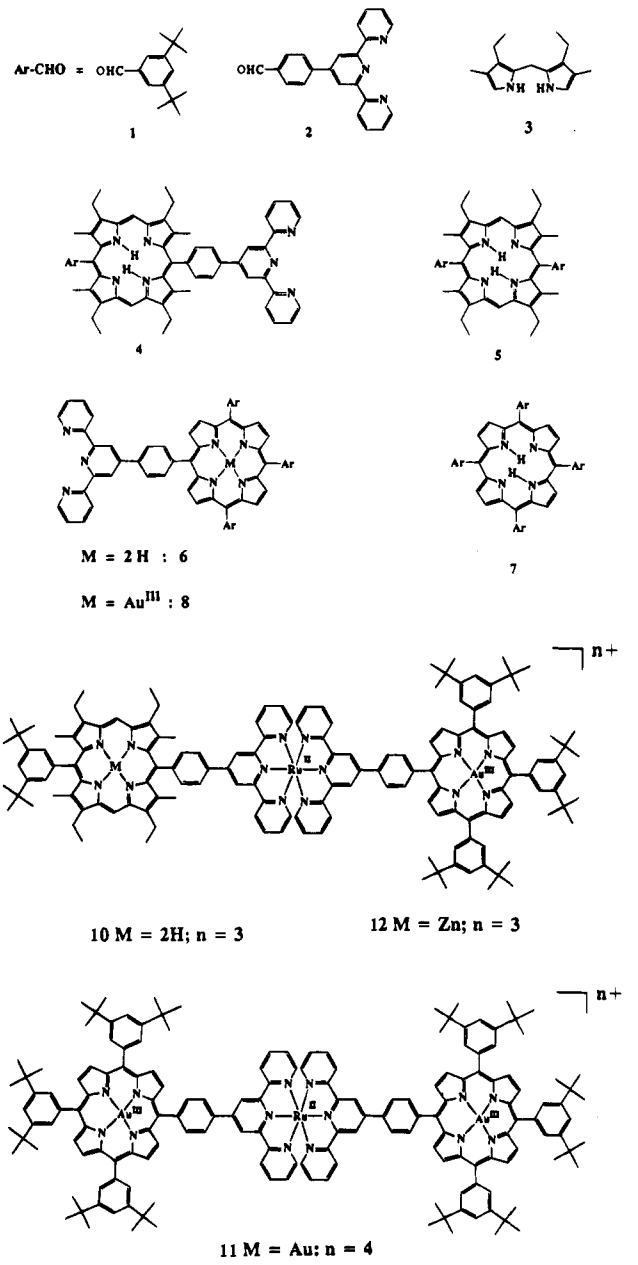

Figure 1. Structures of the various porphyrins and precursors used in the present work.

porphyrinic subunits used in this study, together with relevant precursors, are shown in Figure 1 while the stepwise formation of asymmetrical ruthenium(II) complexes[26] from the respective molecular modules is illustrated in Figure 2. Synthesis of the octaalkyldiarylporphyrin **4** was achieved following McDonald's methodology[27] using Lindsey's conditions[28] for the acid-catalyzed condensation of dipyrrylmethane **3** with aldehydes **1** and **2** in CH_2Cl_2. The tetraarylporphyrin **6** was prepared using both Adler's[29] and Lindsey's[28] methods.

Compounds. 5-[2,2′:6′,2″-Terpyridine]-4′-ylphen-4-yl]-15-(3,5-di-*tert*-butylphenyl)-2,8,12,18-tetraethyl-3,7,13,17-tetramethylporphyrin (4). A 100 mL two-necked round-bottom flask, equipped with a reflux condenser and septum, was charged with bis(3-ethyl-4-methyl-2-pyrryl)methane (**3**) (380 mg, 1.65 mmol), 4′-(4-formylphenyl)-2,2′:

(14) (a) Odobel, F.; Sauvage, J.-P. *New J. Chem.* **1994**, *18*, 1139. (b) Odobel, F.; Sauvage, J.-P.; Harriman, A. *Tetrahedron Lett.* **1993**, *34*, 8113.
(15) Bixon, M.; Jortner, J. *J. Phys. Chem.* **1991**, *95*, 1941.
(16) (a) Marcus, R. A. *J. Chem. Phys.* **1956**, *24*, 966. (b) Marcus, R. A. *J. Chem. Phys.* **1957**, *26*, 867. (c) Marcus, R. A. *Discuss. Faraday Soc.* **1960**, *29*, 21.
(17) (a) Liang, N.; Miller, J. R.; Closs, G. L. *J. Am. Chem. Soc.* **1989**, *111*, 8740. (b) Liang, N.; Miller, J. R.; Closs, G. L. *J. Am. Chem. Soc.* **1990**, *112*, 5353.
(18) Gubelmann, M.; Harriman, A.; Lehn, J.-M.; Sessler, J. L. *J. Phys. Chem.* **1990**, *94*, 308.
(19) Schmidt, E. S.; Calderwood, T. S.; Bruice, T. C. *Inorg. Chem.* **1986**, *25*, 3718.
(20) (a) Hamilton, A. D.; Rubin, H.-D.; Bocarsley, A. B. *J. Am. Chem. Soc.* **1984**, *106*, 7255. (b) Sessler, J. L.; Capuano, V. L.; Burell, A. K. *Inorg. Chim. Acta* **1993**, *204*, 93.
(21) Collin, J.-P.; Harriman, A.; Heitz, V.; Odobel, F.; Sauvage, J.-P. *J. Am. Chem. Soc.* **1994**, *116*, 5679.
(22) Rowley, N. M.; Kurek, S. S.; George, M. W.; Hubig, S. M.; Beer, P. D.; Jones, C.J.; Kelly, J. M.; McCleverty, J. A. *J. Chem. Soc., Chem. Commun.* **1992**, 497.
(23) Newman, M. S.; Lee, L. F. *J. Org. Chem.* **1972**, *26*, 4468.
(24) Guillerez, S. Ph.D. Thesis, Université Louis Pasteur de Strasbourg, France, 1990.
(25) Young, R.; Chang, C. K. *J. Am. Chem. Soc.* **1985**, *107*, 898.
(26) (a) Collin, J.-P.; Guillerez, S.; Sauvage, J.-P.; Barigelletti, F.; De Cola, L.; Flamigni, L.; Balzani, V. *Inorg. Chem.* **1991**, *30*, 4230. (b) Thummel, R. P.; Jahng, Y. *Inorg. Chem.* **1986**, *25*, 2527.
(27) Arsenault, G. P.; Bullock, E.; MacDonald, S. F. *J. Am. Chem. Soc.* **1980**, *82*, 4234.
(28) Lindsey, J. S.; Hsu, H. C.; Schreiman, J. C.; Kearney, P. C.; Marguerettaz, A.M. *J. Org. Chem.* **1987**, *52*, 827.
(29) Adler, A. D.; Longo, F. R.; Finarelli, J. D.; Goldmacher, J.; Assour, J.; Korsakoff, L. *J. Org. Chem.* **1967**, *32*, 476.

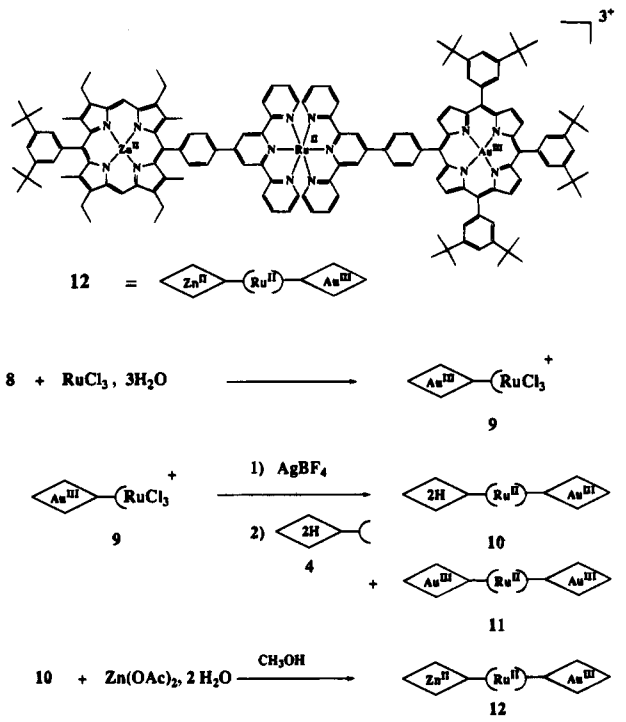

Figure 2. Synthetic strategy used to assemble triad **12**.

6′,2″-terpyridine (**2**) (95 mg, 0.28 mmol), 3,5-di-*tert*-butylbenzaldehyde (**1**) (244 mg, 1.12 mmol), and freshly distilled CH_2Cl_2 (40 mL). The mixture was purged for 15 min with Ar before trifluoroacetic acid (50 μL) was added via a syringe. The flask was covered with aluminum foil and stirred under Ar at room temperature for 15 h to give a red-colored solution. Chloranil (1 g, 4 mmol) was added, and the deep red-colored solution was refluxed for 1 h. After cooling to room temperature, the crude reaction solution was neutralized with 10% aqueous sodium carbonate, and after separating, the organic phase was washed twice with water. Subsequently, the solvent was removed by rotary evaporation, and the red-black residue was purified by column chromatography on alumina. The symmetrical porphyrin 5,15-bis(2,5-di-*tert*-butylphenyl)-2,8,12,18-tetraethyl-3,7,13,17-tetramethylporphyrin (**5**) was first eluted with a mixture of hexane/ethyl acetate (99.5/0.5). The required porphyrin **4** was subsequently eluted from the column with a mixture of hexane/ethyl acetate (97.5/2.5). The porphyrinic products were rechromatographed twice on alumina and recrystallized from CH_2Cl_2/CH_3OH. The [[terpyridine]ylphenyl]porphyrin **4** was isolated in 20% yield while the symmetrical porphyrin **5** was recovered in 30% yield. Data for **4**: ^{1}H NMR (400 MHz, $CDCl_3$) δ = 10.25 (s, 2H); 9.09 (s, 2H); 8.83 (d,d,d, 2H, J = 4.7, 1.8, and 0.8 Hz); 8.80 (d,d,d, 2H, J = 7.9, 1.0, and 1.0 Hz); 8.31 (d, 2H, J = 8.2 Hz); 8.25 (d, 2H, J = 8.2 Hz); 7.97 (d,d,d, 2H, J = 7.9, 7.9, and 1.8 Hz); 7.92 (d, 2H, J = 1.9 Hz); 7.81 (t, 1H, J = 1.9 Hz); 7.43 (d,d,d, 2H, J = 7.6, 4.8, and 1.2 Hz); 4.04 (m, 8H); 2.58 (s, 6H); 2.47 (s, 6H); 1.80 (t, 12 H, J = 7.5 Hz); 1.52 (d, 18H); −2.37 (s, 2H); ES-MS m/z = 974.99 ([$C_{67}H_{71}N_7$ + H^+] requires 974.58); UV−vis (CH_2Cl_2) λ_{max} (log ϵ) = 409 (5.36); 506 (4.25); 540 (3.66); 573 (3.84); 624 (2.98) nm. Data for **5**: ^{1}H NMR (200 MHz, CD_2Cl_2) δ = 10.28 (s, 2H); 7.95 (d, 4H, J = 1.8 Hz); 7.88 (t, 2H, J = 1.8 Hz); 4.07 (q, 8H, J = 7.6 Hz); 2.52 (s, 12H); 1.82 (t, 12H, J = 7.6 Hz); 1.54 (s, 36H); −2.37 (s, 2H); FAB-MS m/z = 855.6 ([$C_{60}H_{78}N_4$ − 1e] requires 855.3), UV−vis (CH_2Cl_2) λ_{max} = 409; 507; 540; 573; 626 nm.

5-[2,2′:6′,2″-Terpyridine]-4′-ylphen-4-yl]-10,15,20-tris(3,5-di-*tert*-butylphenyl)porphyrin (6). Lindsey Method. A 2 L two-necked round-bottom flask, equipped with a reflux condenser and septum, was charged with 4′-(4-formylphenyl)-2,2′:6′,2″-terpyridine (**2**) (250 mg, 0.74 mmol), 3,5-di-*tert*-butylbenzaldehyde (**1**) (2.43 g, 11.1 mmol), and freshly distilled CH_2Cl_2 (1.2 L). The mixture was purged for 15 min with Ar before pyrrole (82 mL, 11.8 mmol) was added, followed by addition of trifluoroacetic acid (200 μL) via a syringe. The flask was covered with aluminum foil and stirred under Ar at room temperature for 14 h to give a red-colored solution. Chloranil (1g, 4 mmol) was added, and the resultant black solution was refluxed for 1 h. Approximately 1 L of the solvent was removed by rotary evaporation under reduced pressure, and after cooling to room temperature, the crude reaction solution was neutralized with 10% aqueous sodium carbonate. After separating, the organic phase was washed three times with aqueous sodium dithionite (0.15 M) and subsequently with water. The solvent was removed by rotary evaporation, and the red-black residue was purified by column chromatography on alumina. The symmetrical porphyrin 5,10,15,20-tetrakis(2,5-di-*tert*-butylphenyl)porphyrin (**7**) was first eluted with a mixture of hexane/ethyl acetate (99.9/0.1). The required porphyrin **6** was then eluted from the column with a mixture of hexane/ethyl acetate (99/1). Porphyrin **6** was rechromatographed twice on alumina before being recrystallized from CH_2Cl_2/CH_3OH and was isolated in 9% yield. The symmetrical porphyrin **7** was rechromatographed on silica gel with CH_2Cl_2/hexane as eluent and was recovered in 11% yield.

Adler Method. A 250 mL round-bottom flask, equipped with a reflux condenser, was charged with 4′-(4-formylphenyl)-2,2′:6′,2″-terpyridine (**2**) (300 mg, 0.90 mmol), 3,5-di-*tert*-butylbenzaldehyde (**1**) (3.52 g, 16.1 mmol), pyrrole (1.18 mL, 17 mmol), and propionic acid (110 mL). The mixture was heated to reflux for 30 min, and after cooling to room temperature, the propionic acid was removed by azeotropic distillation with toluene under reduced pressure. The resulting red-brown solid was dissolved in CH_2Cl_2 and washed twice with 10% aqueous sodium carbonate and three times with water. The organic layer was dried over Na_2SO_4 and evaporated to dryness under reduced pressure. After purification of the crude product by column chromatography as described above, porphyrins **6** and **7** were recovered in yields of 13% and 20%, respectively. Data for **6**: ^{1}H NMR (400 MHz, CD_2Cl_2) δ = 9.11 (s, 2H); 8.96 (d, 2H, J = 4.8 Hz); 8.94 (d, 2H, J = 4.8 Hz); 8.91 (s, 4H); 8.80 (m, 2H); 8.78 (m, 2H); 8.42 (d, 2H, J = 8.3 Hz); 8.24 (d, 2H, J = 8.3 Hz); 8.12 (d, 4H, J = 1.8 Hz); 8.10 (d, 2H, J = 1.8 Hz); 7.97 (d,d,d, 2H, J = 7.6, 7.6, and 1.6 Hz); 7.86 (t, 3H, J = 1.8 Hz); 7.43 (m, 2H); 1.54 (s, 54H); −2.73 (s, 2H); ES-MS m/z = 1183.67 ([$C_{83}H_{87}N_7$ + H^+] requires 1183.67); UV−vis (CH_2Cl_2) λ_{max} (log ϵ) = 422 (5.73); 518 (4.29); 554 (4.07); 593 (3.76); 649 (3.83) nm. Data for **7**: ^{1}H NMR (200 MHz, CD_2Cl_2) δ = 8.90 (s, 8H); 8.15 (d, 8H, J = 1.8 Hz); 7.79 (t, 4H, J = 1.8 Hz); 1.54 (s, 72H); −2.67 (s, 2H); FAB-MS m/z = 1063.7 ([$C_{76}H_{94}N_4$ + H^+] requires 1063.6); UV−vis (CH_2Cl_2) λ_{max} (log ϵ) = 421 (5.71); 518 (4.15); 553 (4.04); 572 (3.70); 648 (3.78) nm.

[5-[2,2′:6′,2″-Terpyridine]-4′-ylphen-4-yl]-10,15,20-tris(3,5-di-*tert*-butylphenyl)porphyrinato]aurate (8). A 150 mL two-necked round-bottom flask, equipped with a reflux condenser and septum, was charged with porphyrin **6** (74 mg, 63 μmol), $KAuCl_4$ (59 mg, 156 μmol), sodium acetate (41 mg, 0.5 mmol), and Ar-purged acetic acid (5 mL). The flask was covered with aluminum foil and heated to reflux for 6 h. Absorption spectroscopy indicated that the characteristic four-banded Q-region of the free-base porphyrin **6** had been replaced with a two-banded Q-region characteristic of a metalloporphyrin. The acetic acid was removed by evaporation under reduced pressure, and the orange-red residue was dissolved in CH_2Cl_2 (250 mL) and washed, under vigorous shaking, with saturated aqueous KPF_6. The organic layer was separated and washed several times with 10% aqueous sodium carbonate and three times with water before being dried over Na_2SO_4. After removal of the solvent under reduced pressure, the crude product was recrystallized from CH_2Cl_2/hexane and chromatographed on alumina with CH_2Cl_2/CH_3OH (9/1) as eluent. Purified **8** was isolated in 85% yield: ^{1}H NMR (400 MHz, CD_2Cl_2) δ = 9.43 (d, 2H, J = 5.3 Hz); 9.40 (d, 2H, J = 5.3 Hz); 9.38 (s, 4H); 9.08 (s, 2H); 8.77 (d,d,d, 2H, J = 4.7, 1.8, and 1.0 Hz); 8.74 (d,d,d, 2H, J = 7.6, 1.0, and 1.0 Hz); 8.42 (s, 4H); 8.13 (d, 4H, J = 1.8 Hz); 8.10 (d, 2H, J = 1.6 Hz); 7.99 (t, 3H, J = 1.6 Hz); 7.96 (d,d,d, 2H, J = 7.6, 7.6, and 2.1 Hz); 7.43 (d,d,d, 2H, J = 7.5, 4.6, and 1.2 Hz); 1.55 (s, 36H); 1.54 (s, 18H); ES-MS m/z = 689.25 ([$C_{83}H_{85}N_7Au^+$ + H^+] requires 689.31); UV−vis (CH_2Cl_2) λ_{max} (log ϵ) = 416 (5.36); 524 (4.25); 564 (shoulder) nm.

Triads 10 and 11. To a 25 mL round-bottom flask was added **8** (54 mg, 35 μmol), $RuCl_3 \cdot 3H_2O$ (12 mg, 45 μmol), and absolute ethanol (5 mL). The mixture was heated to reflux for 3 h in the dark before being cooled overnight at −20 °C. Ethanol was removed under reduced pressure. Attempts to recrystallize the crude product from various solvents and solvent mixtures were unsuccessful, and so the dark red

product, assumed to be **9**, was used without further purification. The product was dissolved in acetone (30 mL) containing ethanol (5 mL) and $AgBF_4$ (23 mg, 0.12 mmol) and refluxed under Ar for 2.5 h in the dark. After cooling to room temperature, the solution was filtered through a PTFE membrane (pore size 0.5 μm), and the resulting deposit of AgCl was washed with acetone. The combined filtrates and washings were added to ethanol (17 mL), and the acetone was removed selectively by rotary evaporation. Subsequently, **4** (34 mg, 35 μmol) was added to the ethanol solution, and the mixture was heated to reflux under Ar for 3 h in the dark. The solvent was evaporated and the residue dissolved in acetonitrile before being subjected to anion exchange. Purification of the crude product was carried out by column chromatography on silica gel. Triad **10** was first eluted from the column with CH_3CN/water/saturated aqueous KNO_3 (95/5/0.02) while triad **11** was removed by subsequent elution with CH_3CN/water/saturated aqueous KNO_3 (95/5/0.04). Further chromatography on silica gel using acetone/water/saturated aqueous KNO_3 (95/5/0.03) as eluent was necessary for both compounds. After anion exchange, triads **10** and **11** were isolated in yields of 25% and 6%, respectively. Data for **10**: ^{1}H NMR (400 MHz, CD_3CN) δ = 10.40 (s, 2H); 9.48 (d, 2H, J = 5.6 Hz); 9.43 (m, 4H); 9.40 (s, 4H); 9.36 (s, 4H); 8.87 (m, 4H); 8.84 (d, 2H, J = 4.2 Hz); 8.71 (d, 2H, J = 8.1 Hz); 8.68 (m, 2H); 8.53 (d, 2H, J = 7.8 Hz); 8.19 (s, 4H); 8.17 (s, 2H); 8.08 (m, 7H); 7.95 (s, 3H); 7.68 (d, 2H, J = 5.3 Hz); 7.63 (d, 2H, J = 5.6 Hz); 7.35 (m, 2H); 7.33 (m, 2H); 4.14 (q, 8H, J = 7.4 Hz); 2.75 (s, 6H); 2.53 (s, 6H); 1.86 (t, 6H, J = 7.5 Hz); 1.83 (t, 6H, J = 7.8 Hz); 1.56 (s, 54H); 1.53 (s, 18H); −2.43 (s, 2H); ES-MS m/z = 614.17 ([$C_{150}H_{156}N_{14}RuAu^{3+}$ + H^+] requires 613.51); UV−vis (CH_2Cl_2) λ_{max} (log ϵ) = 414 (5.69); 495 (4.72); 520 (shoulder); 570 (4.16); 626 (3.42) nm. Data for **11**: ^{1}H NMR (400 MHz, CD_2Cl_2) δ = 9.48 (d, 4H, J = 5.2 Hz); 9.43 (d, 4H, J = 5.2 Hz); 9.40 (s, 4H); 9.36 (s, 8H); 8.86 (d, 4H, J = 8.3 Hz); 8.79 (d, 4H, J = 8.3 Hz); 8.68 (d, 4H, J = 8.2 Hz); 8.19 (d, 4H, J = 1.8 Hz); 8.17 (d, 8H, J = 1.8 Hz); 8.08 (m, 10H); 7.64 (d,d,d, 4H, J = 4.8, 1.4, and 0.8 Hz); 7.33 (d,d,d, 4H, J = 7.4, 7.4, and 1.3 Hz); 1.57 (s, 72H); 1.56 (s, 36H); ES-MS m/z = 714.68 ([$C_{166}H_{170}N_{14}RuAu_2^{4+}$] requires 714.07); UV−vis (CH_2Cl_2) λ_{max} (log ϵ) = 415 (5.76); 493 (4.72); 560 (shoulder) nm.

Triad 12. Triad **10** (16 mg, 5.54 μmol) and zinc acetate dihydrate (5 mg, 22.8 μmol) were dissolved in absolute methanol (10 mL), and the mixture was heated to reflux under Ar for 30 min. The course of reaction was followed by UV−vis spectroscopy until metalation of the free-base porphyrin was complete. After cooling to room temperature, anion exchange was made and the crude product was chromatographed on silica gel using acetone/water/saturated aqueous KNO_3 (95/5/0.03) as eluent. Triad **12** was recovered in 85% yield: ^{1}H NMR (400 MHz, CD_3CN) δ = 10.27 (s, 2H); 9.48 (d, 2H, J = 5.2 Hz); 9.45 (s, 2H); 9.43 (d, 2H, J = 5.2 Hz); 9.40 (s, 2H); 9.36 (s, 4H); 8.87 (m, 4H); 8.79 (d, 2H, J = 8.0 Hz); 8.70 (d, 2H, J = 5.7 Hz); 8.68 (d, 2H, J = 8.3 Hz); 8.52 (d, 2H, J = 7.8 Hz); 8.19 (d, 4H, J = 1.8 Hz); 8.17 (d, 2H, J = 1.8 Hz); 8.08 (m, 7H); 7.94 (d, 2H, J = 1.5 Hz); 7.93 (t, 1H, J = 1.6 Hz); 7.68 (d, 2H, J = 5.3 Hz); 7.63 (d, 2H, J = 5.6 Hz); 7.35 (m, 2H); 7.33 (m, 2H); 4.12 (q, 4H, J = 7.3 Hz); 4.07 (q, 4H, J = 7.6 Hz); 2.70 (s, 6H); 2.48 (s, 6H); 1.85 (t, 6H, J = 7.4 Hz); 1.81 (t, 6H, J = 7.6 Hz); 1.56 (s, 54H); 1.54 (s, 18H); ES-MS m/z = 838.66 ([$C_{150}H_{154}N_{14}RuZnAu^{3+}$ + H^+] requires 838.80); UV−vis (CH_2Cl_2) λ_{max} (log ϵ) = 413 (5.70); 494 (4.72); 525 (4.61); 571 (4.14) nm.

Instrumentation. Cyclic voltammetry was carried out with a Bruker EI310M potentiostat connected to an Ifelec 3802 XY recorder with a three-electrode system; experiments were made with either a Pt wire or a hanging Hg drop as the working electrode, a Pt wire as the auxiliary electrode, and a potassium chloride saturated calomel electrode (SCE) as the reference. The reference electrode was separated from the bulk of the solution by a glass tube fitted to the bottom of the cell with a fine porosity sintered-glass frit immersed in acetonitrile solution containing tetra-*n*-butylammonium tetrafluoroborate (0.1 M). Experiments were carried out at 22 °C in acetonitrile solution containing tetra-*n*-butylammonium tetrafluoroborate (0.1 M) after deoxygenation by purging with Ar for 20 min. Potentials are reported versus SCE. The sweep rate was 100 mV s^{-1}, and the experimental reproducibility was ±10 mV.

Luminescence lifetimes were measured by time-correlated, single-photon counting techniques using a mode-locked, synchronously pumped, cavity-dumped dye laser. The pump source was a frequency-doubled Antares 76S Nd:YAG laser equipped with an energy and spatial stabilizer. Rhodamine 6G and (frequency-doubled) styryl-9 dye lasers were used to provide appropriate excitation wavelengths. Emission was isolated from scattered laser light using glass cutoff filters in conjunction with a high radiance monochromator, and decay profiles were recorded at six distinct wavelengths within the emission band. After deconvolution of the instrumental response function (fwhm = 50 ps) and applying global analysis methodology, the time resolution of this instrument was *ca.* 15 ps. Variable temperature studies were made with the sample cell housed in either a thermostated metal block or a quartz dewar. Temperatures were measured with a thermocouple in direct contact with the sample.

Laser flash photolysis studies were made with a frequency-doubled, mode-locked Nd:YAG laser (pulse width 30 ps, maximum energy 25 mJ/pulse). The primary excitation wavelength (i.e., 532 nm) was modulated so as to provide excitation pulses at 440, 556, or 590 nm by Raman shifting with appropriate high-pressure vapor cells. A white light continuum for use as the analyzing beam was generated by focusing residual 1064 nm output from the laser into CS_2. The monitoring and excitation pulses were directed almost collinearly through the sample cell, with the monitoring pulse being delayed with an optical delay stage. Transient differential absorption spectra were recorded with a Princeton image-intensified, dual-diode array interfaced to a Spex spectrograph. Approximately 300 individual laser shots were averaged for each delay time, and about 50 different delay times were overlaid in order to derive kinetic data. Data analysis was made by computer nonlinear least-squares iteration using global analysis methodology. The ultimate time resolution of this instrument was *ca.* 50 ps.

Improved time resolution was achieved using a frequency-doubled, mode-locked Antares 76S Nd:YAG laser as the excitation pump for a Coherent Model 700 pyromethene dual-jet dye laser. A Quantel Model RGA67-10 regenerative amplifier, a Quantel Model PTA-60 dye laser, and a Continuum Model SPA1 autocorrelator were used to produce pulses with a fwhm of about 300 fs. The spectrometer was run at 10 Hz, and the output pulse was split to produce excitation and monitoring pulses. Output from the pyromethene dye laser was at 556 nm (2 mJ/pulse). The monitoring pulse was delayed with a computerized optical delay stage, and spectra were acquired with a Princeton dual-diode array spectrograph. About 600 individual laser shots were averaged at each time delay, and data analysis was made as above.

Results and Discussion

Excitation into the Ruthenium(II) Bis(terpyridyl) Subunit. Absorption spectra recorded for the three tripartite compounds (Figure 3) are well described as superpositions of spectra of the individual components, without perturbation of the π-electronic systems. In each case, the ruthenium(II) bis(terpyridyl) complex is primarily responsible for absorption around 440−500 nm, where the metal-to-ligand charge-transfer (MLCT) absorption band is the dominant transition. Excitation of triads **10**−**12** in deoxygenated acetonitrile solution at 440 nm gave rise to extremely weak luminescence centered around 640 nm (Figure 4) that retained the same spectral features as observed for ruthenium(II) bis-(4′-tolylterpyridine) used as the reference compound.[30] This emission is attributed, therefore, to luminescence from the MLCT triplet state of the central ruthenium(II) bis(terpyridyl) subunit, although the quantum yields were too low to be measured with meaningful accuracy. The luminescence lifetimes (τ_L) measured for compounds **10**−**12** in deoxygenated acetonitrile solution were on the order of 220 ± 30 ns, being noticeably shorter than that of the reference compound (τ_O = 565 ± 35 ps). This finding indicates that the appended porphyrins quench the triplet excited state of the central metal complex. Following from earlier studies,[21] this

(30) Benniston, A. C.; Harriman, A.; Grosshenny, V.; Ziessel, R. *Angew. Chem., Int. Ed. Engl.* **1994**, *33*, 1884.

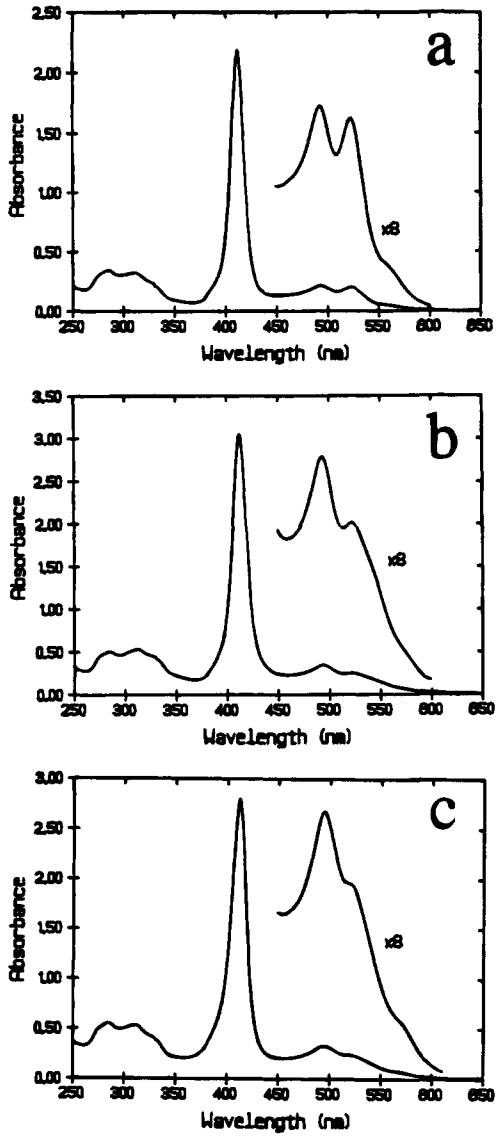

Figure 3. Absorption spectra recorded for (a) **10**, (b) **11**, and (c) **12** in acetonitrile solution.

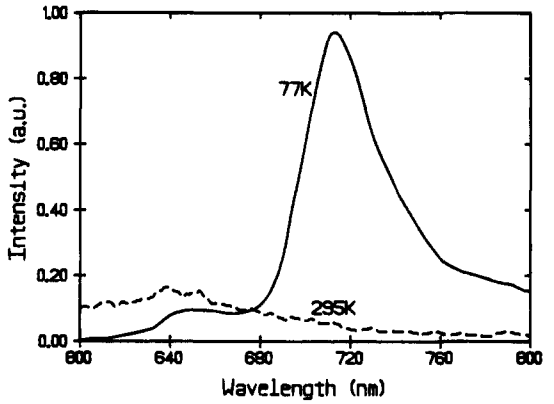

Figure 4. Luminescence spectra recorded for triad **11** in ethanol at 295 K (- - -) and at 77 K (—). The emission centered around 650 nm is attributed to luminescence from the central ruthenium(II) bis(terpyridyl) complex while that centered around 715 nm, seen only at 77 K, is assigned to phosphorescence from the gold(III) porphyrin.

quenching process is attributed to triplet energy transfer to one of the appended porphyrins.

The rates of intramolecular triplet energy transfer ($k_{EN} = [(1/\tau_L) - (1/\tau_O)]$) were found to be comparable for each compound, the average value being *ca.* 3×10^9 s^{-1}. From low-temperature

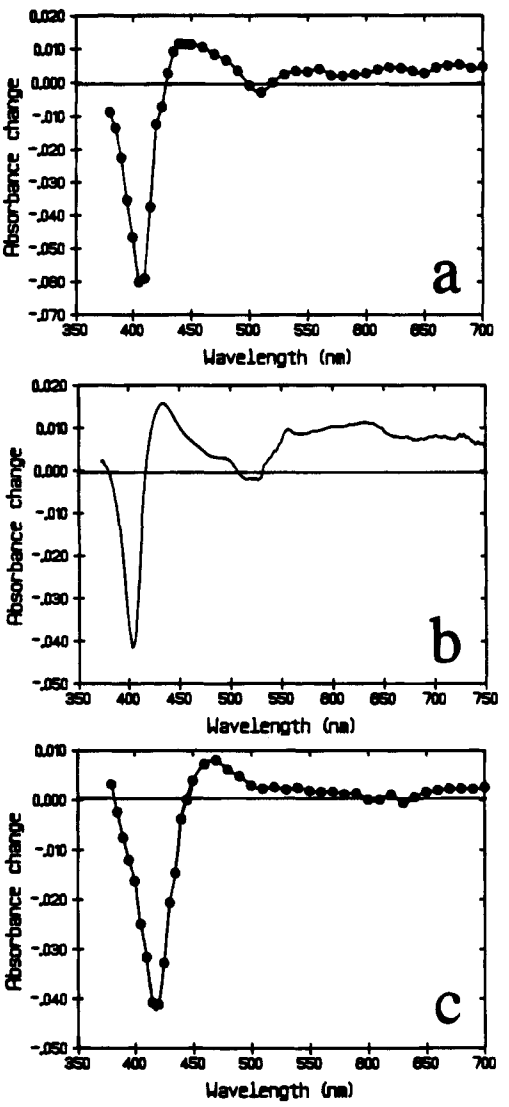

Figure 5. Differential transient absorption spectra recorded after excitation of the ruthenium(II) bis(terpyridyl) subunit of the various triads in deoxygenated acetonitrile solution with a 30 ps laser pulse at 440 nm. The spectra refer to triplet excited states of the (a) free-base porphyrin subunit in **10** recorded 100 ns after the laser pulse, (b) one of the gold porphyrin subunits in **11** recorded 1 ns after the laser pulse, and (c) the zinc porphyrin subunit in **12** recorded 100 ns after the laser pulse.

phosphorescence studies made with the various porphyrin reference compounds, the triplet energy gaps (ΔE_{TT}) were calculated to be 0.17, 0.21, and 0.36 eV, respectively, for transfer to gold(III), zinc(II), and free-base porphyrinic subunits. Laser flash photolysis studies carried out with compounds **10**–**12** in deoxygenated acetonitrile solution showed the presence of triplet excited states associated with the gold(III) porphyrin and, for **10** and **12**, the second porphyrin (Figure 5). Since laser excitation was at 440 nm where the porphyrin is essentially transparent, it follows that these porphyrin triplet states are populated via energy transfer from the central ruthenium(II) bis(terpyridyl) complex.

Intramolecular triplet energy transfer within triads **10**–**12** was also observed to take place in an ethanol glass at 77 K. For compound **11**, the rate of energy transfer was found to be $(2.0 \pm 0.5) \times 10^8$ s^{-1} at 77 K while the lifetime of ruthenium(II) bis(4′-tolylterpyridine) was measured as 10 ± 1 μs under identical conditions. Thus, triplet energy transfer is essentially quantitative at 77 K, and as can be seen clearly from the steady-state luminescence spectrum recorded at 77 K, phosphorescence

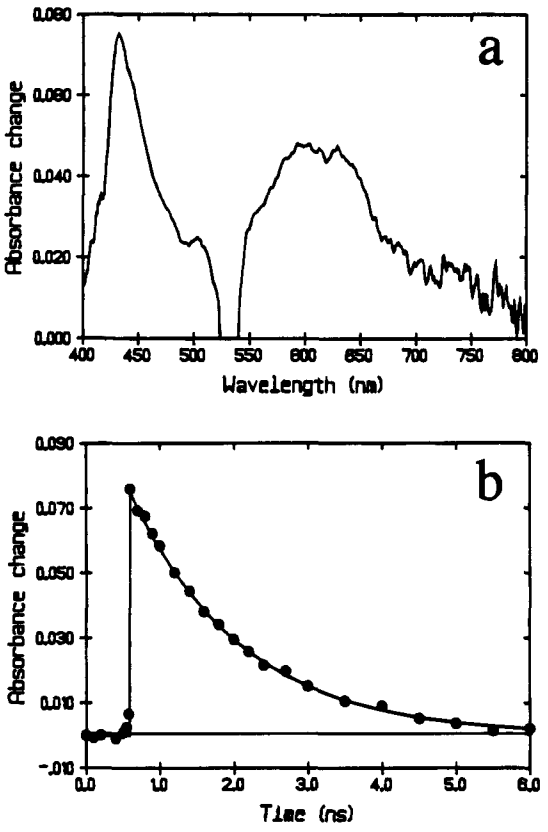

Figure 6. (a) Differential transient absorption spectrum recorded 200 ps after excitation of **11** in acetonitrile solution with a 30 ps laser pulse at 532 nm. (b) Kinetic trace showing decay of the transient species at 440 nm for the above experiment.

from the gold(III) porphyrin subunit can be observed (Figure 4). For the asymmetrical triads **10** ($k_{EN} \approx 1.1 \times 10^8$ s^{-1}) and **12** ($k_{EN} \approx 1.5 \times 10^8$ s^{-1}), triplet energy transfer was also quantitative at 77 K and resulted in formation of extremely long-lived porphyrin triplet excited states.

Reaction of the Excited Triplet States of the Porphyrin Subunits. Excitation of the various tripartite compounds with a 30 ps laser pulse at 532 nm, where the gold(III) porphyrin subunit is the dominant chromophore, resulted in formation of the triplet excited state of the gold(III) porphyrin (Figure 6a). This species, which does not emit in fluid solution, can be readily detected by its characteristic differential absorption spectrum.[13] For each of the triads, and also for the relevant monomeric gold(III) porphyrin **7**−Au$^+$, the triplet lifetime (τ_T) was found to be 1.5 ± 0.2 ns. The triplet state decays cleanly to the prepulse baseline without involvement of any other intermediate species (Figure 6b). In these systems, therefore, the triplet state of the gold(III) porphyrin remains unquenched by either the adjacent ruthenium(II) bis(terpyridyl) complex or the distant second porphyrin. This situation is somewhat surprising, at least at first glance, since triplet energy transfer from the gold(III) porphyrin to both zinc(II) (ΔE_{TT} = 0.04 eV) and free-base (ΔE_{TT} = 0.19 eV) porphyrins is energetically favorable according to low-temperature phosphorescence spectra. Presumably, electron exchange via the central metal complex is too ineffective for triplet energy transfer to seriously compete with the relatively fast nonradiative deactivation of the gold(III) porphyrin excited triplet state ($k \approx 6.7 \times 10^8$ s^{-1}).

Electron transfer from the central ruthenium(II) bis(terpyridyl) complex to the triplet excited state of the gold(III) porphyrin is calculated to be slightly endergonic ($\Delta G° \approx 0.05$ eV):

$$\Delta G° = [E_{OX} - E_{RED} - E_T - (2e^2/4\pi\epsilon_s\epsilon_o R_{cc})] \quad (1)$$

where E_{OX} (=1.25 V vs SCE) refers to the redox potential for one-electron oxidation of the ruthenium(II) bis(terpyridyl) complex, E_{RED} (=−0.59 V vs SCE) refers to the redox potential for one-electron reduction of the gold(III) porphyrin, and E_T (=1.74 eV) is the triplet energy of the gold(III) porphyrin obtained from phosphorescence spectra. The final term in eq 1 (=0.05 eV) corrects for the decrease in Coulombic potential accompanying charge transfer, where ϵ_o is the permittivity of free space, ϵ_s (=37.1) is the static dielectric constant of acetonitrile, and R_{cc} (=14.6 Å) is the center-to-center distance separating the reactants. Thus, electron abstraction from the central metal complex by the gold(III) porphyrin triplet state is not expected to occur within the limited time available.

The zinc(II) (E_{OX} = 0.63 V vs SCE) and free-base (E_{OX} = 0.78 V vs SCE) porphyrin subunits are considerably easier to oxidize than is the central ruthenium(II) bis(terpyridyl) complex. Indeed, electron transfer from the second porphyrin ring to the triplet excited state of the appended gold(III) porphyrin is calculated from eq 1 (with the final term being zero) to be exergonic for both **10** ($\Delta G° = -0.37$ eV) and **12** ($\Delta G° = -0.52$ eV). The large separation distance ($R_{cc} \approx 30$ Å) inherent in these reactions, however, is inconducive for fast electron transfer. Such reactions are unable to compete with nonradiative deactivation of the gold(III) porphyrin triplet state ($k \approx 6.7 \times 10^8$ s^{-1}), and it is clear that the central ruthenium(II) bis(terpyridyl) complex is ineffective at promoting electronic coupling between these reactants. The situation is quite different with 2,9-diphenyl-1,10-phenanthroline as the spacer group, where the triplet state of the gold porphyrin rapidly ($k \approx 8 \times 10^9$ s^{-1}) abstracts an electron from the second porphyrin.[13]

Following excitation of **10** or **12** with a 30 ps laser pulse at 440 nm, the excited triplet states of the free-base or zinc(II) porphyrinic subunits, respectively, were observed on the microsecond time scale (Figure 5). These triplets decayed via first-order kinetics with lifetimes similar to those of the respective monomeric reference compounds. Again, there is no indication in the laser flash photolysis records of electron- or energy-transfer reactions occurring in these systems. Electron-transfer reactions between the adjacent ruthenium(II) bis(terpyridyl) complex and these triplets are thermodynamically unfavorable although electron transfer to the appended gold(III) porphyrin is thermodynamically favorable and has been observed in related systems.[13] The thermodynamic driving force for reduction of the gold(III) porphyrin by the triplet state of **10** ($\Delta G° = -0.18$ eV) and **12** ($\Delta G° = -0.48$ eV) is modest, so that reaction is likely to fall within the normal region of a Marcus-type energy-gap profile.[16,17] Even so, from the measured triplet lifetimes we estimate that the rate constant for intramolecular electron transfer in these systems must be less than *ca.* 10^5 s^{-1}. In the corresponding phenanthroline-bridged systems,[13] electron transfer to the appended gold(III) porphyrin occurs from both free-base ($k = 3 \times 10^3$ s^{-1}) and zinc(II) ($k = 8 \times 10^7$ s^{-1}) porphyrins.

Excitation into the Free-Base Porphyrin Subunit of 10. Excitation of **10** in acetonitrile solution at 595 nm, where the free-base porphyrin subunit is the only chromophore, gave rise to a fluorescence spectrum displaying the characteristic features of a free-base porphyrin. The fluorescence yield measured for **10** was *ca.* 15% that of an optically-matched equimolar mixture of the individual components. Time-resolved fluorescence studies indicated that the fluorescence decay profile recorded for the corresponding free-base porphyrin reference compound **5** was well-described in terms of a single exponential having a

Scheme 1

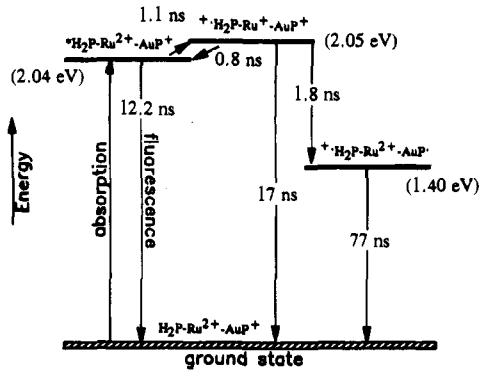

lifetime of 12.2 ± 0.1 ns. In contrast, fluorescence decay profiles recorded for **10** required analysis as the sum of three exponentials:

$$I_F(t) = A_1 \exp(-t/\tau_1) + A_2 \exp(-t/\tau_2) + A_3 \exp(-t/\tau_3) \quad (2)$$

The longest of these three derived lifetimes (i.e., $\tau_3 = 4.6$ ns) contributed less than 1% to the initial fluorescence intensity (i.e., $A_3 < 0.01$). Furthermore, the fractional contribution, but not the lifetime, was found to change markedly with both excitation and monitoring wavelength, although A_3 was always <0.03. This component, therefore, is attributed to a fluorescent impurity. The other two lifetimes ($\tau_1 = 0.59$ ns; $\tau_2 = 2.56$ ns) contributed almost equally to the initial fluorescence intensity (see the supporting information) and their relative fractional contributions remained independent of excitation and monitoring wavelength. Gated fluorescence spectra recorded for the two components, as resolved by their temporal difference, were identical and consistent with that expected for a free-base porphyrin. Thus, these two components are assigned to the excited singlet state of the free-base porphyrin subunit in **10**.

In order to better understand the origin of this dual-exponential behavior, time-resolved fluorescence studies were made in acetonitrile solution over a modest temperature range. At all temperatures, the fluorescence decay profiles required analysis in terms of eq 2, with A_3 remaining <0.03 and with $\tau_3 = 4.6 \pm 0.2$ ns throughout the data set. The other two lifetimes (see the supporting information) decrease with increasing temperature, accompanied by a progressive increase in the significance of the shorter-lived species. This behavior is consistent with the model presented in Scheme 1. Here, excitation at 595 nm results in quantitative formation of the first excited singlet state of the free-base porphyrin subunit. A charge-transfer reaction takes place, in competition with the inherent radiative and nonradiative deactivation processes, in which an electron is transferred from the excited singlet state to the appended ruthenium(II) bis(terpyridyl) complex:

$$*(H_2P)-Ru^{2+}-(AuP^+) \rightarrow (^{\bullet+}H_2P)-Ru^{+}-(AuP^+) \quad (3)$$

Provided the thermodynamic driving force for light-induced charge transfer is negligible, electron transfer becomes reversible and the decay profiles should acquire dual exponentiality:

$$(^{\bullet+}H_2P)-Ru^{+}-(AuP^+) \rightarrow *(H_2P)-Ru^{2+}-(AuP^+) \quad (4)$$

In fact, the thermodynamic driving force for the forward reaction can be estimated from cyclic voltammetry studies and fluorescence spectra according to

$$\Delta G^\circ = [E_{OX} - E_{RED} - E_S - (e^2/4\pi\epsilon_s\epsilon_o R_{cc})] \quad (5)$$

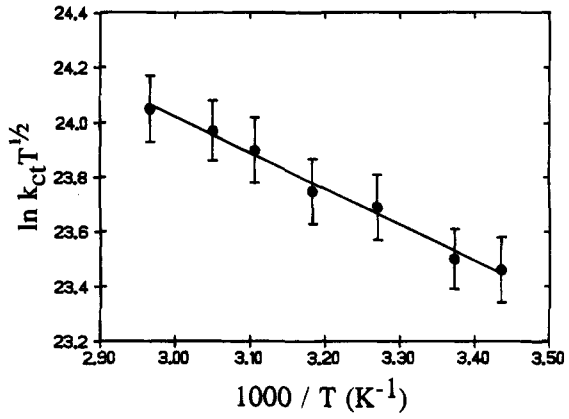

Figure 7. Effect of temperature on the rate of photoinduced charge transfer measured for triad **10** in acetonitrile solution. The line drawn through the experimental points corresponds to a least-squares fit to the Marcus expression with an activation energy of 0.113 eV.

where E_{OX} (=0.78 V vs SCE) refers to the redox potential for one-electron oxidation of the free-base porphyrin subunit, E_{RED} (=−1.24 V vs SCE) refers to the redox potential for one-electron reduction of the central ruthenium(II) bis(terpyridyl) complex, and E_S (=1.98 eV) is the singlet excitation energy of the free-base porphyrin subunit. The center-to-center separation corresponds to 14.6 Å so that the final term in eq 5 has a value of only 0.025 eV. On this basis, $\Delta G^\circ = 0.015$ eV and, consequently, charge transfer is expected to be highly reversible.

Analysis of the time-resolved fluorescence data in terms of Scheme 1 permits calculation[12,31] of the rates of forward (k_{CT}) and reverse (k_{-CT}) charge-transfer processes (see the supporting information). The thermodynamic driving force for charge transfer at room temperature derived from the kinetic analysis ($\Delta G^\circ = 0.008$ eV) is in excellent agreement with that obtained above from electrochemical measurements ($\Delta G^\circ = 0.015$ eV). Expressing the derived ΔG° values in terms of the Gibbs–Helmholtz equation allows estimation of the reaction enthalpy change ($\Delta H^\circ = 0.17$ eV) and entropy change ($\Delta S^\circ = 0.000\,54$ eV K^{-1}).

The derived rates of forward charge transfer increase with increasing temperature and can be expressed in terms of the Marcus equation for nonadiabatic electron transfer:[16]

$$k_{CT} = (4\pi^2/h)(V_{DA})^2(4\pi k_B T\lambda)^{-1/2} \exp[-E_A/RT] \quad (6)$$

$$E_A = (\lambda + \Delta G^\circ)^2/4\lambda \quad (7)$$

From the observed temperature dependence (Figure 7), the activation free energy change (E_A) was calculated to be 0.11 eV. Using the derived ΔG° values and assuming that the reorganization energy (λ) remains insensitive to temperature over the range studied, the best fit to eq 6 was obtained with $\lambda = 0.50$ eV and $V_{DA} = 15$ cm^{-1}. Both values are modest, and in particular, the magnitude of V_{DA} indicates relatively weak electronic coupling between the subunits, despite their close proximity. The total reorganization energy can be partitioned[3b,16] into terms associated with the solvent reorganization energy (λ_s) and with the nuclear reorganization energy (λ_v) that describes any change in structure accompanying charge transfer. The former term can be estimated from dielectric continuum theory:[32]

(31) Heitele, H.; Finckh, P.; Weeren, S.; Pöllinger, F.; Michel-Beyerle, M. E. *J. Phys. Chem.* **1989**, *93*, 5173.
(32) Marcus, R. A. *Can. J. Chem.* **1959**, *37*, 155.

$$\lambda_s = 0.6[e^2/4\pi\epsilon_o]\{(1/2R_A) + (1/2R_B) - (1/R_{CC})\}\{(1/n^2) - (1/\epsilon_s)\} \quad (8)$$

where R_A (=6.2 Å) and R_B (=6.0 Å) refer, respectively, to the molecular radii of the porphyrin and the ruthenium(II) bis(terpyridyl) subunits, and n is the refractive index of the solvent. In eq 8, the integer (=0.6) is a geometry factor that corrects the dielectric continuum model for the molecular architecture of the compound under investigation.[33,34] The average value found for λ_s (=0.43 eV) indicates that this term dominates the total reorganization energy such that charge transfer causes only a small structural distortion. Even so, this is a small solvent reorganization energy when compared to most other photosynthetic models,[5,13] and it was further observed that the rates of forward charge transfer were relatively insensitive to changes in solvent polarity (see the supporting information).

According to Scheme 1, secondary charge-transfer processes might be expected to compete with reverse charge transfer to restore the excited singlet state of the free-base porphyrin. Thus, charge recombination (k_{CR}) can regenerate the ground state ($\Delta G°$ = −2.00 eV),

$$(^{\bullet+}H_2P)-Ru^+-(AuP^+) \rightarrow (H_2P)-Ru^{2+}-(AuP^+) \quad (9)$$

while a charge-shift reaction (k_{CS}) can occur in which the intermediate ruthenium(I) bis(terpyridyl) complex [more correctly described as the ruthenium(II) bis(terpyridyl) π-radical anion] reduces the appended gold(III) porphyrin ($\Delta G°$ = −0.65 eV).

$$(^{\bullet+}H_2P)-Ru^+-(AuP^+) \rightarrow (^{\bullet+}H_2P)-Ru^{2+}-(AuP^{\bullet}) \quad (10)$$

Detailed analysis of the time-resolved fluorescence decay records[12,31] allows determination of the sum of the rate constants for these two electron-transfer steps ($k_{SUM} = k_{CR} + k_{CS}$); the derived values are given as supporting information. The temperature dependence for this overall rate constant corresponds to an activation energy of 0.13 eV, but the data cannot be partitioned into individual rate constants. As above, it was noted that the combined rates of these secondary electron-transfer reactions were not significantly dependent upon the polarity of the solvent (see the supporting information), possibly indicating a small solvent reorganization energy.

Laser flash photolysis studies were found consistent with the excited singlet state of the free-base porphyrin subunit being present immediately after excitation of **10** in acetonitrile solution at room temperature with a 30 ps laser pulse at 590 nm (Figure 8). This species decayed over several nanoseconds via complex kinetics to leave a residual transient absorption signal. This latter signal partially decayed with a first-order rate constant of $(1.3 \pm 0.1) \times 10^7$ s^{-1} while the remaining signal decayed with a lifetime of 20 ± 5 μs at low laser intensity. The longest-lived species can be identified from its differential absorption spectrum, quenching by molecular oxygen, and self-quenching at high laser intensity as the triplet excited state of the free-base porphyrin. It originates from the inherent intersystem-crossing process of the incompletely quenched singlet excited state.

The intermediate species possessing a lifetime of 75 ± 5 ns is attributed to the charge-transfer state in which an electron has been transferred from the free-base porphyrin to the appended gold(III) porphyrin. A similar species was characterized previously for a molecular dyad having the free-base and gold(III) porphyrins separated by a 2,9-diphenyl-1,10-phenanthroline spacer moiety.[13] From the known molar extinction coefficients of the various species,[13] it was estimated that this charge-transfer state was formed with a quantum yield of 0.27 ± 0.04. On this basis, rate constants for charge recombination and charge shift are calculated to be 6×10^7 and 5.6×10^8 s^{-1}, respectively, at room temperature. This relative order seems in accord with Marcus theory[16] if the two reactions involve comparable electronic coupling matrix elements since, assuming λ = 0.50 eV for both processes, charge recombination should lie deeper into the Marcus inverted region than the less exergonic charge-shift reaction.

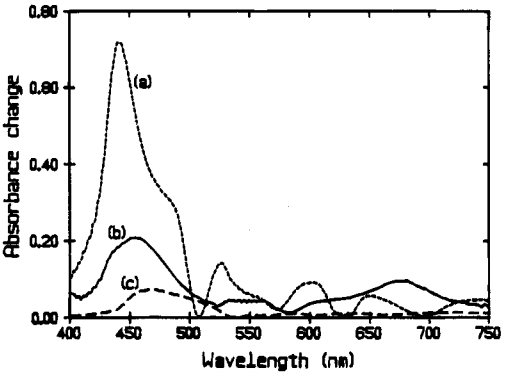

Figure 8. Differential transient absorption spectra recorded (a) 30 ps, (b) 15 ns, and (c) 200 ns after excitation of **10** in acetonitrile solution with a 30 ps laser pulse at 590 nm.

Excitation into the Zinc(II) Porphyrin Subunit of 12. Excitation of **12** at 556 nm, where the zinc(II) porphyrin subunit is the dominant chromophore, gave rise to weak fluorescence having the same spectral profile as that recorded for the monomeric zinc porphyrin reference compound **5**−Zn. The fluorescence lifetime (τ_s) measured in acetonitrile solution at 25 °C was found to be 50 ± 6 ps, compared to a value (τ_f) of 2.2 ± 0.1 ns recorded for the reference compound under identical conditions. Unlike the situation found for **10**, fluorescence decay profiles were well described in terms of a single-exponential component. The extensive fluorescence quenching found for this system, together with the simpler fluorescence decay kinetics, appears consistent with a larger thermodynamic driving force for electron transfer from the excited singlet state to the appended ruthenium(II) bis(terpyridyl) complex:

$$*(ZnP)-Ru^{2+}-(AuP^+) \rightarrow (^{\bullet+}ZnP)-Ru^+-(AuP^+) \quad (11)$$

In fact, from eq 5 with E_{OX} = 0.63 V vs SCE and E_s = 2.09 eV, the Gibbs free energy change for forward charge transfer is calculated as $\Delta G°$ = −0.25 eV. Fluorescence quenching is attributed, therefore, to intramolecular charge transfer, for which the rate constant ($k_{CT} = [(1/\tau_s) - (1/\tau_f)] = 2 \times 10^{10}$ s^{-1}) can be calculated from the fluorescence lifetimes measured for **12** (τ_s) and for **5**−Zn (τ_f). The same reaction occurs in the absence of the appended gold(III) porphyrin,[21] where the rate of forward charge transfer ($\Delta G°$ = −0.28 eV) was found to be 3.6×10^{10} s^{-1}:

$$*(ZnP)-Ru^{2+} \rightarrow (^{\bullet+}ZnP)-Ru^+ \quad (12)$$

Bearing in mind that the edge-to-edge separation distance between the reactants in these systems is only *ca.* 7 Å and that, following from the analysis made with **10**, charge transfer involves only a modest reorganization energy ($\lambda \approx$ 0.50 eV), these rates seem to be relatively slow. In fact, for the corresponding system having a rhodium(III) bis-

(33) Walker, G. C.; Barbara, P. F.; Doorn, S. K.; Dong, Y.; Hupp, J. T. *J. Phys. Chem.* **1991**, *95*, 5712.

(34) The magnitude of the integer was determined from low-temperature fluorescence studies as described later in the text.

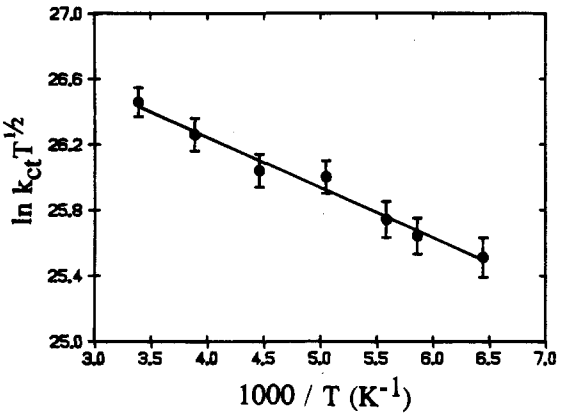

Figure 9. Effect of temperature on the rate of photoinduced charge transfer measured for triad **12** in ethanol solution. The line drawn through the experimental points corresponds to a least-squares fit to the Marcus expression with an activation energy of 0.026 eV.

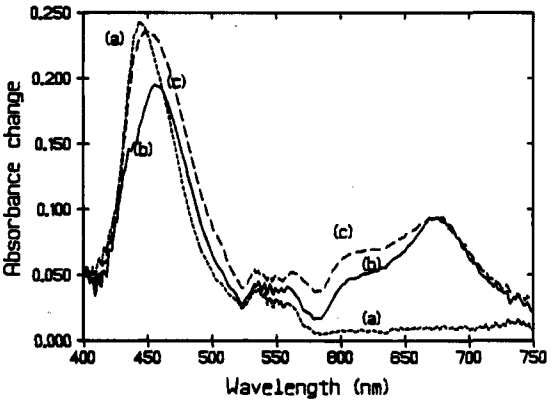

Figure 10. Differential transient absorption spectra recorded (a) 2 ps, (b) 200 ps, and (c) 10 ns after excitation of **12** in acetonitrile solution with a 1 ps laser pulse at 556 nm.

(terpyridyl) complex linked to the porphyrin[21] it was observed that omitting the bridging phenyl ring gave a substantial increase in the rate of charge transfer. The most likely culprit causing the slow rate of charge transfer in **12**, therefore, is the orthogonally-oriented phenyl ring that connects the reactants.[35,36]

Time-resolved fluorescence studies were carried out in ethanol solution over a wide temperature range, and the effect of temperature on the rate of charge transfer (k_{CT}) is depicted in Figure 9. The apparent activation energy derived from this study is 0.026 eV. Assuming charge transfer for both **10** and **12** is characterized by a common entropy factor, which seems reasonable in view of their similar structures, and allowing for the known temperature effect on the dielectric properties of ethanol,[37] the total reorganization energy accompanying charge transfer at 25 °C is calculated from this plot to be *ca.* 0.45 eV. This value is very similar, if not identical, to that determined for **12** ($\lambda \approx 0.50$ eV) and is dominated by the solvent reorganization energy ($\lambda_s \approx 0.33$ eV), as calculated from eq 8. From the intercept to Figure 9 and on the basis of the applicability of eq 6 to this system, the electronic matrix coupling element V_{DA} is estimated to be *ca.* 12 cm^{-1}. This is a small value, comparable to that derived for **12** ($V_{DA} = 15$ cm^{-1}), which indicates the relatively poor electronic communication between the excited-state chromophore and the central metal complex in these triads.

Laser flash photolysis studies were made with **12** in deoxygenated acetonitrile solution at 25 °C (Figure 10) in order to elicit more information about the reaction mechanism. Immediately after excitation at 556 nm with a subpicosecond laser pulse the characteristic differential absorption spectrum[13] of the zinc porphyrin excited singlet state can be observed (Figure 10). This species decays with a lifetime of 45 ± 7 ps, in good agreement with the value determined by time-resolved fluorescence spectroscopy, to generate the zinc porphyrin π-radical cation (Figure 10). Deactivation of the excited singlet state, therefore, is attributed to charge transfer to the adjacent ruthenium(II) bis(terpyridyl) complex (Scheme 2). This process is followed by a charge-shift reaction in which the distant gold(III) porphyrin is reduced (Figure 10). The rate constant for

Scheme 2

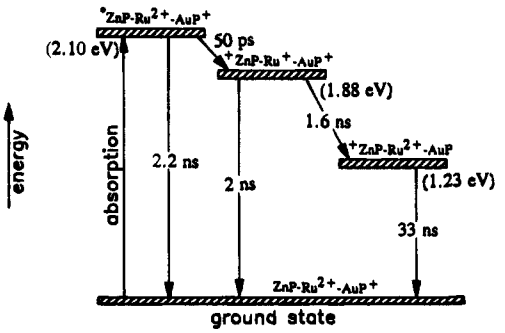

this latter process, derived by monitoring the growth of the reduced gold(III) porphyrin, was found to be $(7 \pm 2) \times 10^8$ s^{-1}. This value is in excellent agreement with that determined ($k = 5.6 \times 10^8$ s^{-1}) for the same process occurring in the free-base porphyrin-containing triad **10**:

$$(^{\bullet+}\text{ZnP})-\text{Ru}^{+}-(\text{AuP}^{+}) \rightarrow (^{\bullet+}\text{ZnP})-\text{Ru}^{2+}-(\text{AuP}^{\bullet}) \quad (13)$$

$$(^{\bullet+}\text{ZnP})-\text{Ru}^{+}-(\text{AuP}^{+}) \rightarrow (\text{ZnP})-\text{Ru}^{2+}-(\text{AuP}^{+}) \quad (14)$$

The charge-shift reaction ($\Delta G° \approx -0.65$ eV) competes favorably with charge recombination to restore the ground state ($\Delta G° \approx -1.88$ eV) since the former occurs close to the apex of a Marcus-type plot ($-\Delta G° \approx 1.4\lambda$) while the latter is well into the inverted region ($-\Delta G° \approx 4\lambda$). The quantum yield for formation of the inter-porphyrin charge-transfer state was estimated from the flash photolysis records to be 0.60 ± 0.05, a value that appears to confirm the contention that the inefficiency of triad **10** stems from the reversibility of the light-induced charge-transfer step.

The lifetime of the inter-porphyrin charge-transfer state was found to be 33 ± 5 ns. This value is somewhat shorter than that found for triad **10** but still much longer (i.e., 55-fold) than that for the corresponding phenanthroline-bridged system.[13] Inter-porphyrin charge recombination for **12** occurs on the same time scale as we would expect[38] to find spin rephasing, so it is possible that the radical pair acquires some triplet character. The shorter lifetime found for **12** relative to **10** might be associated with the smaller energy gap for the zinc porphyrin-containing triad ($\Delta G° \approx 1.22$ eV) since charge recombination might occur slightly closer to the apex of a Marcus-type plot ($-\Delta G° \approx 1.7\lambda$).

(35) Helms, A.; Heiler, D.; McLendon, G. *J. Am. Chem. Soc.* **1991**, *113*, 4325.

(36) (a) Heiler, D.; McLendon, G.; Rogalskyj, P. *J. Am. Chem. Soc.* **1987**, *109*, 604. (b) Helms, A.; Heiler, D.; McLendon, G. *J. Am. Chem. Soc.* **1992**, *114*, 6227. (c) Osuka, A.; Maruyama, K.; Mataga, N.; Asahi, T.; Yamazaki, I.; Tamai, N. *J. Am. Chem. Soc.* **1990**, *112*, 4958.

(37) *Landolt-Bornstein*, 6 Auf., II Band 6 Teil; Springer-Verlag: Berlin, 1959.

(38) Wasielewski, M. R.; Norris, J. R.; Bowman, M. K. *Faraday Discuss. Chem. Soc.* **1984**, *78*, 279.

Photoinduced Charge Transfer for Triad 12 in the Solid State at 77 K. There was no observable fluorescence quenching upon excitation into the free-base porphyrin subunit in triad **10**, compared to the relevant reference porphyrin **5**, in an ethanol glass at 77 K. In contrast, the fluorescence quantum yield measured following excitation into the zinc(II) porphyrin subunit in triad **12** was only *ca.* 20% that found for the corresponding reference porphyrin **5**−Zn under identical conditions. Time-resolved fluorescence decay profiles recorded for **12** in ethanol at 77 K required analysis as the sum of two exponentials with lifetimes of 0.25 ns (82%) and 1.3 ns (18%). On the basis of this dual exponentiality arising from reversible charge transfer (Scheme 1), rate constants for forward and reverse charge-transfer steps, respectively, were derived to be 3.1×10^9 and 1.3×10^9 s^{-1} in the frozen glass. These rate constants can be used to determine the Gibbs free energy change associated with forward charge transfer as being $\Delta G^\circ = -0.006$ eV. In turn, this derived free energy change can be used to indicate that the charge-transfer state is destabilized by *ca.* 0.25 eV in the frozen glass relative to acetonitrile solution at room temperature. The magnitude of this destabilization energy (ΔE_D) can be related to differences in the static dielectric constant of frozen ethanol ($\epsilon_G = 3.0$)[39] and fluid acetonitrile ($\epsilon_s = 37.1$)[40] according to the following expression:[41]

$$\Delta E_D = \sigma[e^2/4\pi\epsilon_o]\{(1/2R_A) + (1/2R_B) - (1/R_{CC})\}\{(1/\epsilon_G) - (1/\epsilon_s)\} \quad (15)$$

where the parameter σ is a geometry factor that corrects the dielectric continuum model for a more exact description of the molecular system and the other terms have been defined earlier. For the above case, $\sigma = 0.6$, a value seemingly consistent with the relative insensitivity of the rate of charge transfer to changes in the solvent dielectric constant (see the supporting information).

The destabilization energy derived for **12** is only *ca.* 30% that found for related molecular dyads.[11,12] This finding can be attributed to the close spacing between the subunits and to the relatively large size of the reactants. These architectural features, together with the avoidance of subunits that undergo substantial geometry changes upon oxidation or reduction (e.g., benzoquinones), also serve to minimize the reorganization energy that accompanies charge transfer. The precise meaning of the geometry factor σ is more difficult to define, however, as is the significance of dealing with a charge-shift reaction rather than a formal charge-separation process. Moreover, it is clear that application of a simple dielectric continuum model that treats the reactants as spheres is inappropriate for such complicated structures.

Using time-resolved fluorescence spectroscopy, the rate of photoinduced charge transfer was measured for **12** in an ethanol glass over a modest temperature range (i.e., $77 < T < 125$ K). From the activation energy ($E_A = 0.0325$ eV) derived from the linear Arrhenius plot and assuming that $\Delta G^\circ \approx 0$ eV over this temperature range, the total reorganization energy associated with charge transfer in the frozen glass was estimated from eq 7 to be *ca.* 0.13 eV. From eq 8 the solvent reorganization energy under these conditions is estimated to be *ca.* 0.05 eV such that the nuclear component accounts for most of the reorganization energy in the frozen glass. With this value in hand, the electronic coupling matrix element V_{DA} was calculated from eq 6 to be *ca.* 17 cm^{-1}. This latter term is within experimental error of that determined at room temperature ($V_{DA} = 12$ cm^{-1}) and indicates the absence of significant structural changes, or a change in the electron-transfer pathway, upon cooling. The different reorganization energies noted at 77 and 195 K can be explained in terms of variations in the dielectric properties of the solvent, and it is important to note that ΔG° remains less than λ upon freezing. Charge transfer, therefore, still occurs in the Marcus normal region, and the rate is expected to decrease with decreasing temperature. In fact, the relatively slow rate of charge transfer observed at 77 K ($k_{CT} \approx 3 \times 10^9$ s^{-1}) is due almost entirely to the decreased temperature since the calculated rate constant in an (hypothetical) ethanol glass at 295 K ($k_{CT} \approx 6 \times 10^{10}$ s^{-1}) is similar to that observed in fluid ethanol at 295 K ($k_{CT} \approx 2 \times 10^{10}$ s^{-1}).

The time-resolved fluorescence decay profiles recorded for **12** in an ethanol glass at 77 K were analyzed as before in order to estimate the rate constant for deactivation of the initially-formed charge-transfer state.[12,31] The derived rate constant ($k_{SUM} = 6.7 \times 10^7$ s^{-1}) is about an order of magnitude smaller than the rate constant for charge shift from the reduced metal complex to the terminal gold(III) porphyrin measured in acetonitrile solution at room temperature ($k_{CS} \approx 6 \times 10^8$ s^{-1}). In fact, we would expect k_{CS} to be somewhat lower in the glass because of the reduced driving force (see below). Laser flash photolysis studies performed with the frozen glass confirmed formation of the inter-porphyrin charge-transfer state. This species decayed with a lifetime of 2.5 ± 0.5 μs and, using extinction coefficients measured at room temperature, was formed with a quantum efficiency of 0.40 ± 0.08. Thus, inter-porphyrin charge transfer occurs slowly ($k \approx 4 \times 10^5$ s^{-1}) under these conditions, and the reaction must occur deep in the Marcus inverted region ($-\Delta G^\circ \gg \lambda$).

In fact, the energy level for this spatially-separated, charge-transfer state (E_{CTS}) was estimated to be *ca.* 1.65 eV by addition of the destabilization energy ($\Delta E_D = 0.43$ eV), calculated from eq 15 for $R_A = R_B = 6.2$ Å and with $R_{CC} = 30$ Å, to the room temperature energy gap measured by cyclic voltammetry ($E_{CTS} = 1.22$ eV). This increased energy gap, together with the decreased reorganization energy, pushes inter-porphyrin charge recombination deeper into the inverted region ($-\Delta G^\circ \approx 13\lambda$), thereby helping to increase the lifetime of the charge-transfer state relative to that found at room temperature. Because of the slow rate of charge recombination, it is likely that intersystem crossing to a triplet radical pair[38] occurs, as observed for the phenanthroline-bridged system.[12] This process might further enhance the lifetime of the charge-transfer state. These various energy changes also lower the driving force for the charge-shift reaction that reduces the gold(III) porphyrin ($\Delta G^\circ \approx -0.47$ eV) and pushes this process well into the Marcus inverted region ($-\Delta G^\circ \approx 4\lambda$).

Comparison of Triad 12 with the Photosynthetic Reaction Center Complex. Reaction center complexes of photosynthetic bacteria (RC) provide for a cascade of electron-transfer steps that span the cytoplasmic membrane.[42] The primary photoreaction, which occurs with unitary quantum yield (ϕ), involves electron transfer ($k \approx 3 \times 10^{11}$ s^{-1})[2] between porphyrin-like chromophores that are separated by an edge-to-edge distance (R_{EE}) of 9.5 Å and embedded in a protein matrix.[1] The thermodynamic driving force for the charge-separation process ($\Delta G_{CS}^\circ \approx -0.39$ eV)[3] is almost exactly balanced by the reorganization energy ($-\Delta G^\circ \approx \lambda$)[16] so that the activation

(39) Kevan, L. *Adv. Radiat. Chem.* **1974**, *4*, 181.
(40) Murov, S. L. *Handbook of Photochemistry*; Marcel Dekker: New York, 1973.
(41) Johnson, D. G.; Svec, W. A.; Wasielewski, M. R. *Isr. J. Chem.* **1988**, *28*, 193.
(42) *The Photosynthetic Reaction Center Complex: Structure and Dynamics*; Breton, J., Vermeglio, A., Eds.; Plenum Press: New York, 1988.

energy is at a minimum and the rate is essentially temperature independent.[4] The electronic coupling matrix element for the RC has been estimated[43] as $V_{DA} \approx 25$ cm^{-1} while the rate of the inherent charge-recombination step[3] is *ca.* 2×10^7 s^{-1}. The driving force for this latter process ($\Delta G_{CR}° \approx -0.9$ eV)[3] is such that the reaction falls well within the Marcus inverted region ($-\Delta G° \approx 3.6\lambda$).[16] The relative slowness of charge recombination permits charge-shift reactions to occur in which the redox equivalents become widely spaced (i.e., 70 Å).[42] An additional interesting feature of the primary electron-transfer event is that a neighboring bacteriochlorophyll molecule, which lies just off the most direct pathway,[1] is available as a superexchange mediator.[44]

Many elegant model systems[5-9,13,21] have been constructed in an effort to mimic some of the essential features of the RC. Perhaps the most impressive of these systems has an extended length of *ca.* 80 Å while the ultimate charge-separated state is formed with an overall quantum yield of 83% and survives for 55 μs at room temperature.[45] One obvious advantage of the present approach to building artificial photosynthetic ensembles concerns our use of preformed modules that are assembled around a metal cation.[14] This noncovalent strategy, which is more specific than association via electrostatic[46] or van der Waals interactions[47] and provides for more stable structures than those produced via multipoint hydrogen bonding,[48] might facilitate construction of multicomponent assemblies possessing attractive optical and redox properties. However, the performance of triad **12** is inferior to that of the natural photosystem and to the above-mentioned supermolecular system.[45] In an effort to design more efficacious systems, we have compared the properties evaluated for **12** with those summarized above for the natural system (Table 1).

In describing the performance of triad **12**, we have categorized the charge-transfer reactions as referring to light-induced electron transfer from the singlet excited state of the zinc porphyrin to the adjacent ruthenium(II) bis(terpyridyl) complex (step I) and to subsequent electron transfer from the resultant ruthenium(I) bis(terpyridyl) complex to the appended gold(III) porphyrin (step II). It can be seen that **12** compares remarkably well with the RC with respect to step I for both the forward electron-transfer step and charge recombination (Table 1). The initial rate (k_{CS}) is slower than found in the RC, partly because reaction occurs well within the Marcus normal region ($-\Delta G_{CS}° < \lambda$), but the quantum yield for formation of electron-transfer products is still unitary. The activationless rate constant calculated at $-\Delta G_{CS}° = \lambda$ (k_{ACT}) is an order of magnitude smaller for **12** than for the RC due to less pronounced electronic coupling between the reactants. This is most probably due to the poorly-oriented phenyl bridge. It is reasonable to suppose that both $\Delta G_{CS}°$ and V_{DA} could be tuned by simple synthetic means.

Table 1. Comparison of the Electron-Transfer and Thermodynamic Data Collected for Triad **12** with Those of the Photosynthetic Reaction Center Complex

event	RC[a]	**12**, step I[b]	**12**, step II[c]
	Charge Separation		
ϕ	1.0	1.0	0.60
k (s^{-1})	3×10^{11}	2×10^{10}	7×10^8
$\Delta G_{CS}°$ (eV)	−0.39	−0.25	−0.65
R_{CC} (Å)	17	14.6	14.6
R_{EE} (Å)	9.5	7	7
V_{DA} (cm^{-1})	25	12	3
$-\Delta G_{CS}°/\lambda$	~1	0.5	1.3
k_{ACT} (s^{-1})	3×10^{11}	3×10^{10}	1×10^9
	Charge Recombination		
k (s^{-1})	2×10^7	5×10^8	3×10^7
$\Delta G_{CR}°$ (eV)	−0.9	−1.90	−1.22
R_{CC} (Å)	17	14.6	30
R_{EE} (Å)	9.5	7	20
$-\Delta G_{CR}°/\lambda$	~3.6	4	1.7
$k_{20Å}$ (s^{-1})	1×10^3		3×10^7

[a] *Rhodopseudomonas viridis* reaction center complex with data taken from refs 1−4 and 42−44. [b] Reduction of the central ruthenium(II) bis(terpyridyl) complex and subsequent charge recombination to restore the ground state. [c] Electron transfer from the π-radical anion of the ruthenium(II) bis(terpyridyl) complex to the appended gold(III) porphyrin and subsequent inter-porphyrin charge recombination.

Step II does not compare so well with the RC (Table 1). Electronic coupling between the reactants is much weaker in the model system, and this results in both a slower rate of electron transfer and a lower yield of spatially-separated redox products. The activationless rate constant is now *ca.* 300-fold lower than for the RC due to restricted electronic coupling. Here, the bridging phenyl ring can rotate more freely than is the case with step I so that the reduced V_{DA} term most probably arises from abnormally small atomic orbital coefficients associated with electron tunneling through the bridge. Because we have not found such problems in other systems possessing the same phenylporphyrin modules,[13,21] we may consider that there is very poor coupling at the terpyridine end of the chain. However, it has been demonstrated that there is effective electronic coupling between polyphenyl-linked terpyridyl ligands,[49] and it may be that the real problem is related to electron tunneling across the metal bis(terpyridyl) complex with its orthogonally-sited ligands.[24b]

An additional problem with step II concerns the relatively high rate of interporphyrin charge recombination. This situation is properly exposed by comparing the rate measured for **12** with that estimated[3] for the RC if the reactants were separated by an edge-to-edge distance of 20 Å ($k_{20Å}$). In this case, there is a 10000-fold difference in the rate of charge recombination between the two systems. The rate of inter-porphyrin charge recombination is only 10-fold smaller than that for charge recombination in step I, despite the vastly increased separation distance (Table 1). Several factors combine to cause this high rate of interporphyrin charge recombination, including the poorly-optimized thermodynamic properties ($-\Delta G_{CR}° \approx 1.3\lambda$) which place the reaction nearer to the apex of a Marcus-type energy gap profile. For electron-transfer reactions that occur in the inverted region, it is necessary to consider the implications of quantum mechanical tunneling,[50] since this can markedly affect the Franck−Condon term.[16] In this respect, it is likely that the magnitudes of the electron-vibration coupling strength (S_Δ), a term that describes how well certain high-frequency

(43) (a) Deisenhofer, J.; Michel, H. *Angew. Chem., Int. Ed. Engl.* **1989**, *28*, 829. (b) Huber, R. *Angew. Chem., Int. Ed. Engl.* **1989**, *28*, 848.

(44) Plato, M.; Möbius, K.; Michel-Beyerle, M. E.; Bixon, M.; Jortner, J. *J. Am. Chem. Soc.* **1988**, *110*, 7279.

(45) Gust, D.; Moore, T. A.; Moore, A. L.; Lee, S.-J.; Bittersmann, E.; Luttrull, D. K.; Rehms, A. A.; DeGraziano, J. M.; Ma, X. C.; Gao, F.; Belford, R. E.; Trier, T.T. *Science* **1990**, *248*, 199.

(46) (a) Vergeldt, F. J.; Koehorst, R. B. M.; Schaafsma, T. J.; Lambry, J.-C.; Martin, J.-L.; Johnson, D. G.; Wasielewski, M. R. *Chem. Phys. Lett.* **1991**, *182*, 107. (b) Segawa, H.; Takehara, C.; Honda, K.; Shimidzu, T.; Asahi, T.; Mataga, N. *J. Phys. Chem.* **1992**, *96*, 503. (c) Brun, A. M.; Harriman, A.; Hubig, S. M. *J. Phys. Chem.* **1992**, *96*, 254.

(47) (a) Benniston, A. C.; Harriman, A.; Philp, D.; Stoddart, J. F. *J. Am. Chem. Soc.* **1993**, *115*, 5298. (b) Benniston, A. C.; Harriman, A. *Angew. Chem., Int. Ed. Engl.* **1993**, *32*, 1459.

(48) (a) Harriman, A.; Kubo, Y.; Sessler, J. L. *J. Am. Chem. Soc.* **1992**, *114*, 388. (b) Sessler, J. L.; Wang, B.; Harriman, A. *J. Am. Chem. Soc.* **1993**, *115*, 10418.

(49) Sauvage, J.-P.; Collin, J.-P.; Chambron, J.-C.; Guillerez, S.; Coudret, C.; Balzani, V.; Barigelletti, F.; De Cola, L.; Flamigni, L. *Chem. Rev.* **1994**, *94*, 993.

(50) Jortner, J. *J. Am. Chem. Soc.* **1980**, *102*, 6676.

vibrational modes are coupled to the electron-transfer event, differ markedly for natural and artificial systems,[44] and even for steps I and II. The significance of this term is that it determines how rapidly the rate of electron transfer decreases with increasing energy gap in the inverted region. It has been reported[44] that $S_\Delta \approx 0.5-1$ for the RC, but this value might be somewhat higher for the model compound, ensuring that the rate of charge recombination remains high even at large $-\Delta G_{CR}°/\lambda$ ratios.

It is also necessary to consider that step II and the RC are characterized by disparate attenuation factors (β) that describe how rapidly the rate of electron transfer decreases with increasing separation distance. For the RC,[3] $\beta \approx 1$ Å^{-1}, but a much lower value seems to be in order for inter-porphyrin charge recombination in **12** where the interspersed medium is largely aromatic in character. At first sight, the concept of fast inter-porphyrin charge recombination seems inconsistent with the notion of weak electronic coupling between the π-radical anion of the ruthenium(II) bis(terpyridyl) complex and the gold(III) porphyrin, as proposed above. This apparent discrepancy can be rationalized, however, if the charge-shift reaction occurs via electron transfer but inter-porphyrin charge recombination takes place via hole transfer. This is because the central ruthenium(II) cation is more amenable to oxidation than reduction such that the relevant d-orbitals present a larger energy gap for electron transfer than for hole transfer.

Concluding Remarks

In common with several other model systems,[5-8,45-48] the molecular triads described here possess some interesting features. In particular, the unique molecular architecture permits **12** to undergo highly-efficient photoinduced electron transfer in a low-temperature glass while the modular approach used to assemble the triads is considered to be highly versatile and synthetically appealing.[14] The relatively short lifetime of the inter-porphyrin charge-transfer state can be overcome by attaching a further electron acceptor to the gold(III) porphyrin, thereby extending the sequence of electron-transfer steps. Similarly, the rate of the charge-shift reaction (i.e., step I) might be increased simply by raising the driving force via synthetic means;[51] in fact, this may be the key to formulating improved model systems. The advantage of using a two-step process, as opposed to a single (long) electron-transfer event, to achieve long-range charge separation is clearly evident by comparing singlet- and triplet-state properties of the zinc porphyrin subunit. The triplet is unreactive, but the singlet, with its ability to reduce the interspersed metal complex, is an excellent sensitizer. That the triplet is unreactive toward electron transfer is bothersome since it can be readily populated by intramolecular energy transfer from the central metal complex. It is likely that its relative inertness could be changed, however, by adjusting the thermodynamic driving force. An unfavorable orientation of one of the bridging phenyl rings serves to lower the rate of light-induced electron transfer, a feature that can be overcome by changing the nature of the donor porphyrin, but there is a further hindrance to electron transfer across the supermolecule. This may involve d-orbitals on the metal center itself and, if so, might be more difficult to cure.

Acknowledgment. This work was supported by the NSF (Grant CHE 9102657), NATO (Grant 920916), and the CNRS. The award of a grant from the DOE allowing construction of the femtosecond laser spectrometer is gratefully acknowledged. We thank J.-P. Collin for many helpful discussions and J.-D. Sauer for recording the NMR spectra.

Supporting Information Available: Tables of lifetimes, fractional amplitudes, and derived rate constants for electron transfer measured for triad **10** in acetonitrile at different temperatures, and of lifetimes for the zinc porphyrin excited singlet state in triads **10** and **12** measured in solvents of differing polarity (3 pages). This material is contained in many libraries on microfiche, immediately follows this article in the microfilm version of the journal, can be ordered from the ACS, and can be downloaded from the Internet; see any current masthead page for ordering information and Internet access instructions.

JA942804I

(51) DeGraziano, J. M.; Liddell, P. A.; Leggett, L.; Moore, A. L.; Moore, T. A.; Gust, D. *J. Phys. Chem.* **1994**, *98*, 1758.